Alsaif, A., Garcia, R., Figueiredo, F.P., Neocleous, K., Christofe, A., Guadagnini, M. and Pilakoutas, K., 2019. Fatigue performance of flexible steel fibre reinforced rubberised concrete pavements. Engineering Structures, 193, 170-183. https://doi.org/10.1016/j.engstruct.2019.05.040

Fatigue Performance of Flexible Steel Fibre Reinforced Rubberised Concrete Pavements

Abdulaziz Alsaif[a,b*], Reyes Garcia[a,c], Fabio P. Figueiredo[a], Kyriacos Neocleous[d], Andreas Christofe[d], Maurizio Guadagnini[a], Kypros Pilakoutas[a]

[a] Department of Civil and Structural Engineering, The University of Sheffield, Sir Frederick Mappin Building, Mappin Street, Sheffield, S1 3JD, UK.
[b] Department of Civil Engineering, King Saud University, P. O. Box 800, Riyadh 11421, Saudi Arabia.
[c] School of Engineering, The University of Warwick, Library Road, Coventry, CV4 7AL, UK.
[d] Department of Civil Engineering and Geomatics, Cyprus University of Technology, Achilleos 1 Building, Saripolou 2-8, P.O.Box 50329, 3603 Limassol, CY, Cyprus.

Corresponding author: email: asaalsaif1@sheffield.ac.uk; Tel: +44 (0) 114 222 5729,

Abstract

Recycled rubber particles and steel fibres from end-of-life tyres have the potential to enhance the flexibility and ductility of concrete pavements and produce more sustainable pavement solutions. However, the fatigue behaviour of such pavements is not fully understood. This article investigates the mechanical and fatigue performance of steel fibre reinforced concrete (SFRC) and steel fibre reinforced rubberised concrete (SFRRuC). Specimens tested were cast using rubber particles as replacement of natural aggregates (0%, 30% and 60% by volume), and using a blend of manufactured and recycled tyre steel fibres (40 kg/m^3). Prisms were subjected to four-point flexural cyclic load (f=15 Hz) at stress ratios of 0.5, 0.7, 0.8 and 0.9. The results show that, compared to plain concrete, the addition of steel fibres alone improves the fatigue stress resistance of concrete by 11% (at 25% probability of failure). The replacement of natural aggregates with rubber particles improves the flexibility of SFRRuC (from 51 GPa elastic modules for plain concrete to 13 GPa for SFRRuC), but reduces its fatigue stress resistance by 42% (at 25% probability of failure). However, a probabilistic analysis of the fatigue life data and overall design considerations show that the flexible SFRRuC can be used for pavements. To account for the effect of fatigue load, the Concrete Society approach included in TR34 is modified to account for SFRRuC pavements. Finite element analyses show that flexible SFRRuC pavements can accommodate large subgrade movements and settlements and result in much smaller cracks (up to 24 times) compared to SFRC pavements.

Keywords: *Rubberised concrete; Fatigue performance; Steel fibre reinforced rubberised concrete; Flexible concrete pavement; Recycled fibres*

1 Introduction

Rigid concrete pavements are widely used in the construction of long-lasting roads as they enable a better distribution of load over the subgrade and require overall smaller structural depth, compared to flexible asphalt pavements. However, road pavement slabs are subjected to continuous cyclic traffic and thermal loads that can deteriorate the material mechanical properties, propagate cracks and eventually cause fatigue fracture [1-3], leading to premature pavement failure. A potential solution to enhance the flexibility, toughness and fatigue resistance of concrete pavements is to replace part of the natural aggregates with waste tyre rubber (WTR) particles [4, 5]. Rubber aggregates are known to reduce stiffness and enhance impact and skid resistance of concrete [6-12], but can cause significant decrease in mechanical properties, especially at high rubber contents (up to 90% reduction in compressive strength for 100% natural aggregates replacement) [13-17]. Consequently, until now rubberise concrete (RuC) is mainly utilised in low-strength non-structural applications, e.g. concrete pedestrian blocks [11]. Few researchers studied the performance of RuC in structural applications and to date there are limited studies on the fatigue performance of RuC [7, 18-23]. Liu et al. [7] studied the effect of replacing small percentages of fine natural aggregates with crumb rubber particles (0 to 15% by volume) and found that the fatigue performance of the RuC mixes was better than that of ordinary concrete. The enhancement was attributed to the ability of rubber to resist crack propagation by filling internal spaces and absorbing energy through deformation.

To enhance the strength of RuC for structural applications (especially flexural strength), steel fibres can be used to produce steel fibre reinforced rubberised concrete (SFRRuC) [5, 20, 24-26]. In SFRRuC, rubber particles absorb energy and enhance the fracture characteristics of the material [14, 27], whereas the fibres control crack opening and propagation even after the peak load, thus dissipating energy through gradual fibre debonding [8]. Ganesan et al. [20] examined the flexural fatigue behaviour of self-compacting RuC (SCRuC) with and without manufactured steel fibres. They observed that the replacement of fine aggregates with crumb rubber particles (up to 20% by volume) improved the flexural fatigue strength by approximately 15%. The addition of crimped-type manufactured steel fibres (MSF) into SCRuC mixes further enhanced the fatigue strength by 10%. More recently, Gupta et al. [22] reported that the incorporation of rubber ash and rubber fibres in concrete as a replacement of fine natural aggregates (up to 35% by volume) enhanced the flexural impact and fatigue resistance by up to 217% and 52%, respectively.

Whilst these studies examined the fatigue of mixes with small amounts of rubber (less than 20% by total aggregate volume), recent research [8] has proven that the use of large amounts of rubber (especially large rubber particles) is necessary to attain low stiffness pavements with the potential to accommodate subgrade movements. The authors [8] have recently proposed optimised flexible SFRRuC mixes with large amounts of rubber (60% by volume replacement of natural aggregates) and blends of MSF and recycled tyre steel fibres (RTSF) that meet the flexural strengths of EN 13877-1 [28]. The authors [29, 30] also demonstrated that the durability, long-term and permeability performance indicators of the optimised mixes, rank them as 'highly durable concrete'[31-34]. These properties make SFRRuC a promising candidate for sustainable road pavement slabs, particularly considering that reusing end-of-life tyre materials (WTR and RTSF) in concrete would contribute to the reduction of the environmental impact caused by discarded tyres (1.5 billion units/year [35]). However, to date, the flexural fatigue performance of SFRRuC with large amounts of rubber and steel fibres has not been investigated.

As the variability in flexural fatigue performance of steel fibre reinforced concrete (SFRC) and SFRRuC is expected to be high due to the combination of rubber and/or fibres [20, 22], a statistical approach may need to be adopted to quantify the reliability of experimental results and their suitability for use in pavement design. Probabilistic distribution models including the two-parameter Weibull distribution model, graphical interpolation model and the mathematical model are commonly used to statistically analyse fatigue life data and derive probabilistic relationships that can be used in design [1, 36, 37].

This study assesses the mechanical and fatigue performance of SFRRuC. Initially, the study examines the mechanical performance of SFRC and SFRRuC mixes with different replacement volumes of rubber aggregates (0, 30 and 60%) and a blend of MSF and RTSF. The results are compared in terms of uniaxial compressive strength, static flexural strength, elastic modulus, and flexural fatigue strength (number of fatigue cycles). Subsequently, three different probabilistic approaches are used to estimate the fatigue life. The design implications of using SFRRuC in new pavements is shown by a practical example. Finite element analyses are performed using Abaqus® to demonstrate the capability of flexible SFRRuC pavements to accommodate subgrade movements and settlements. This study contributes towards developing economically and structurally sound alternative materials for sustainable flexible concrete pavements, as well as towards using recycled materials derived from end-of-life tyres.

2 Experimental programme

2.1 Materials and casting procedure

Four optimised concrete mixes developed previously by the authors [8, 11, 29] were produced to cast the tested specimens. Three cubes (100 mm) and twelve prisms (100×100×500 mm) were cast and prepared for each mix. A binder made of 80% of a Portland limestone cement CEM II-52.5 N, 10% of silica fume (SF) and 10% of pulverised fuel ash (PFA) was used for all concrete mixes. The fine aggregate was medium-grade washed river sand with size 0/5 mm and specific gravity (SG) of 2.65, whereas the coarse aggregate was round river washed gravel with particle sizes of 5/10 mm and 10/20 mm and SG of 2.64. Chemical admixtures including plasticiser and superplasticiser were utilised to enhance workability and cohesion. A blend of 20 kg/m^3 of MSF (0.8, 55) and 20 kg/m^3 of RTSF (0.22, 23), as shown in Figure 1a, were used as reinforcement. Details on the characterisations of the steel fibres are reported in [8, 38].

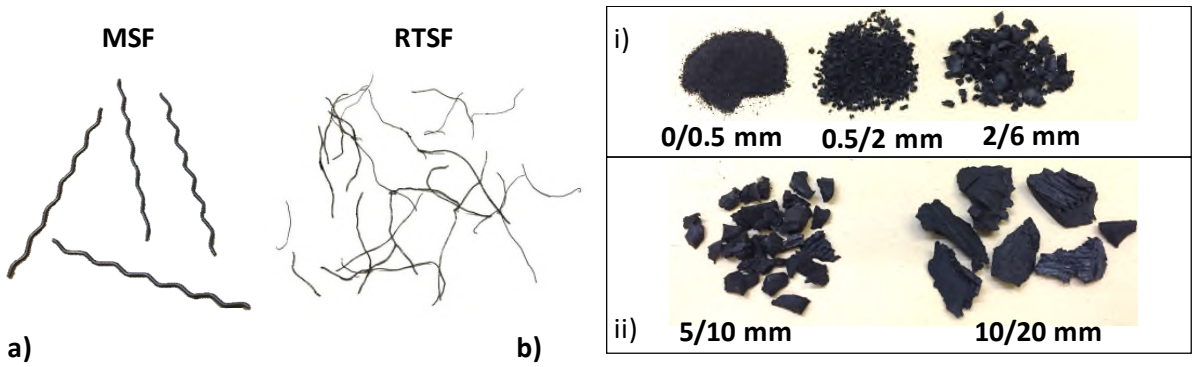

Figure. 1 a) MSF and RTSF, b) rubber particles, used in this study

The natural aggregates were replaced with two different volumetric percentages of rubber particles (30% or 60%) of roughly similar size distribution to minimise packing issues. Figure 1b shows the rubber particles according to size. The fine rubber particles of sizes 0/0.5 mm, 0.5/2 mm and 2/6 mm were used in a 2:3:4 ratio, respectively, whilst the coarse rubber particles of sizes of 5/10 mm and 10/20 mm were used in a 1:1 ratio. The mass of rubber replacing the mineral aggregates was calculated using a relative density of 0.8 [8]. Figure 2 shows the particle size distribution of rubber and natural aggregates (NA) obtained according to ASTM-C136 [39].

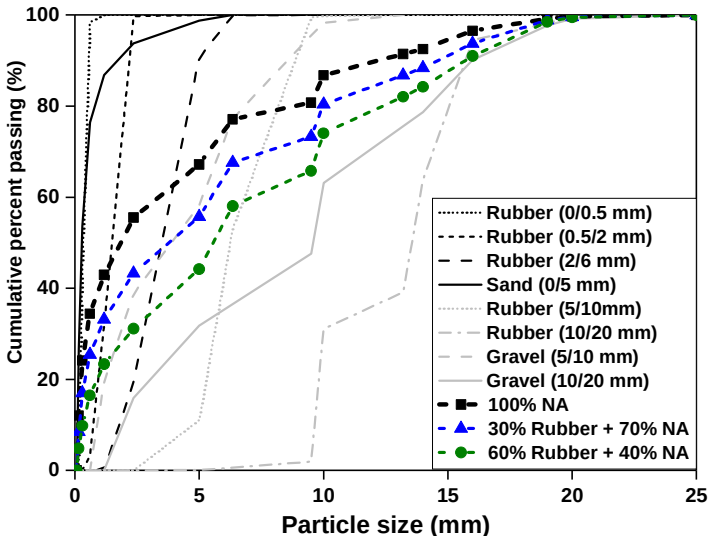

Figure. 2 Particle size distributions for rubber particles and natural aggregates

Table 1 summarises the mix proportions and corresponding IDs of the four concrete mixes examined in this study. The number in the ID represents the quantity of rubber particles replacing both fine and coarse aggregates (0%, 30% or 60% by volume), while P=Plain concrete and BF=blend fibres.

Table 1. Mix proportions for 1 m^3 of concrete, adapted from [8]

Components	Concrete mixes ID			
	0P	*0BF*	*30BF*	*60BF*
CEM II (kg/m^3)	340	340	340	340
Silica Fume (SF) (kg/m^3)	42.5	42.5	42.5	42.5
Pulverised Fuel Ash (PFA) (kg/m^3)	42.5	42.5	42.5	42.5
Fine aggregates 0/5 mm (kg/m^3)	820	820	574	328
Coarse aggregates 5/10 mm (kg/m^3)	364	364	254	146
Coarse aggregates 10/20 mm (kg/m^3)	637	637	446	255
Water (l/m^3)	150	150	150	150
Plasticiser (l/m^3)	2.5	2.5	3.25	4.25
Superplasticiser (l/m^3)	5.1	5.1	5.1	5.1
Fine rubber particles (kg/m^3)	0	0	165	330
Course rubber particles (kg/m^3)	0	0	24.8	49.6
MSF (kg/m^3)	0	20	20	20
RTSF (kg/m^3)	0	20	20	20
Total	2404	2444	2087	1733

To produce the SFRRuC mixes, natural and rubber aggregates were first added into a pan mixer and mixed for approximately 30 s in dry conditions. Half of the mixing water was then added, and the materials were mixed for 1 min. The mixer was halted for three minutes to add the

binder materials. Subsequently, mixing restarted and the remaining water and admixtures were gradually added for another 3 min. Finally, the steel fibres were added manually, and mixing continued for 3 min. All specimens were cast in moulds using two layers of concrete (according to EN 12390-2 [40]), and each layer was compacted on a vibrating table for 25 s. Following casting, the specimens were covered with plastic sheets to retain moisture, and kept under standard laboratory conditions for 2 days. As a large number of specimens were needed for each mix, due to parallel durability studies [29, 30], three batches were cast for each mix. The number of specimens per mix was also limited by the capacity of the concrete mixer in the laboratory. All specimens were cured in a mist room for 28 days, after which they were stored under standard laboratory conditions until testing. All specimens were tested after 150 days following casting to ensure that they had developed their full strength.

2.2 Test setup and instrumentation

The uniaxial compressive tests on cubes were carried out using a cube crusher at a loading rate of 0.4 MPa/s, according to EN 12390-3 [41]. The prisms were subjected to static and fatigue four-point bending using a servo-hydraulic actuator with a capacity of 250 kN (±0.05% error). Two linear variable differential transducers (LVDTs) mounted onto each side of a yoke, as suggested by the JSCE guidelines [42] (see Figure 3), monitored the vertical mid-span displacement of the prisms. The static tests were performed at a displacement rate of 0.2 mm/min. Initially, three prisms per mix were tested statically to select the load limits for the fatigue tests and to monitor the development of cracks. The maximum amplitude of the fatigue load was calculated by multiplying a stress ratio (S=0.5, 0.7 or 0.9) by the average flexural strength obtained from the three specimens subjected to static load. As discussed in more detail in section 3.3, in some cases the stress ratio was multiplied by the characteristic flexural strength (instead of the average) to prevent premature failure of the prisms during the fatigue tests. The minimum amplitude of each loading cycle was set to 10% of the maximum fatigue load to avoid disengagement of the specimens during testing. The fatigue loading cycles were applied at a frequency of 15 Hz (sinusoidal wave), which is within the typical range (12-20 Hz) used for prism tests in order to avoid amplification or resonance problems [1, 19, 36, 43, 44]. The load cycles were applied in four point bending, ensuring a sufficient constant moment region to allow the development of cracked sections at a known stress level. The fatigue tests were terminated either after two million cycles, or at failure of the prisms. Readings were saved at specific logarithmic steps as following (every cycle from 0 to 10 then every10th cycle up to 100 cycles, then every 100th cycle up to 1,000 cycles, then every 1,000th cycle up to 10,000

cycles, then every 10,000th cycle up to failure). The main output of the fatigue tests was the number of cycles at failure as well as the vertical displacements recorded by the LVDTs.

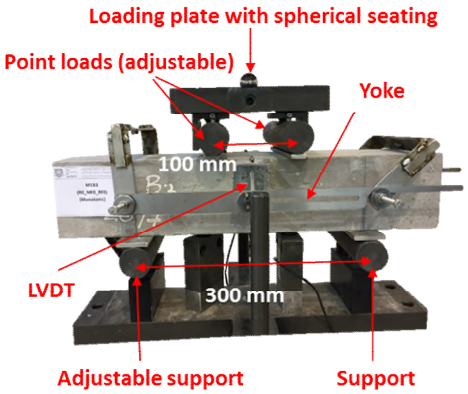

Figure. 3 Flexural test set-up

3 Results and discussion

3.1 Failure mode

Typical failure modes of the tested cubes are shown in Figure 4. Whilst the plain concrete specimens (*0P*) failed in a brittle manner, the SFRC and SFRRuC specimens failed in a much more 'ductile' manner. As the inclusion of large amounts of rubber and steel fibres led to the development of more distributed (and thinner) cracking, compared to specimens without rubber (*0BF*), this confirms that ductility was improved by adding fibres and further enhanced by the rubber, as explained previously by the authors in [8].

Figure. 4 Typical failure modes of concrete cubes

3.2 Static compressive and flexural strengths

Table 2 summarises the average cube compressive strength ($f_{cm,cube}$), static flexural elastic modulus (E_s), and static flexural strength ($f_{ctm,fl}$) including characteristic values ($f_{ctk,fl}$) for each concrete mix. The coefficient of variation is also presented in brackets. The results in Table 2 indicate that the addition of a blend of steel fibres in conventional concrete (mix *0BF*) increases the compressive strength by 18% over the plain concrete mix (*0P*). A similar enhancement was observed in a previous study by the authors [8], who attributed the enhancement to the ability

of steel fibres (especially RTSF) to control and delay micro-crack coalescence and the unstable propagation of cracking. However, mixes *0BF* and *0P* show the same elastic modulus and flexural strength despite the difference in compressive strength, which may be attributed to some air being trapped during the casting of *0BF* prisms as observed by the authors in another study [8]. Indeed, the results in [8] showed that the increase in air content creates weaknesses inside the concrete matrix and decreases concrete density, which in turn affects both the strength and stiffness. Compared to mix *0P*, replacing large amounts of fine and coarse aggregates with rubber reduces the compressive strength by 49% and 85% for *30BF* and *60BF* mixes, respectively. Similarly, the elastic modulus and flexural strength of mix *30BF* drop by 57% and 34%, respectively, whereas these properties decrease by 75% and 42% for mix *60BF*. Nevertheless, in the design of road pavements, which work essentially in bending, having sufficient flexural strength is more important than having high compressive strength, provided durability is not compromised.

Table 2. Static compressive and flexural test results

Mix	$f_{cm,cube}$ (MPa)	E_s (MPa)	$f_{ctm,fl}$ (MPa)	$f_{ctk,fl}$ (MPa)	$\frac{f_{ctm,fl}}{\sqrt{f_{cm,cube}}}$
0P	102 (4.7)	51 (5.1)	7.0 (13.3)	5.2	0.693
0BF	120 (2.9)	51 (4.8)	7.0 (9.3)	5.8	0.639
30BF	52 (7.5)	22 (13.8)	4.6 (5.3)	4.1	0.638
60BF	15 (10.7)	13 (21.9)	4.1 (18.5)	2.6	1.058

The reduction in strength and stiffness in SFRRuC is mainly due to the lower stiffness and higher Poisson's ratio of rubber (nearly 0.5) when compared to natural aggregates, but also due to the poor adhesion between rubber and cement paste [8, 11, 15]. It should be noted that the compressive strength of the mixes degrades faster than the flexural strength, which confirms, as also discussed in [8], that the combination of fibres and rubber enhances the tensile capacity of SFRRuC. This is evident by noting that the ratio of the average static flexural strength to the square root of the average compressive strength ($\frac{f_{ctm,fl}}{\sqrt{f_{cm,cube}}}$) for *60BF* is much higher than for the other mixes.

It should be mentioned that the relatively large variability in $f_{ctm,fl}$ in Table 2 can be attributed to the fact that each specimen belonged to a different batch. To determine a safe initial loading protocol for the fatigue stress loads, the characteristic flexural strength ($f_{ctk,fl}$) of each mix was determined according to RILEM TC 162-TDF [45].

3.3 Flexural fatigue strength

Table 3 summarises the flexural fatigue results of the tested prisms. The results report the stress ratio (S) in decreasing order, as well as the fatigue life (N). For the initial tests (3 prisms per mix), the maximum and minimum amplitudes of the fatigue load were determined using the characteristic strength values ($f_{ctk,fl}$) and S=0.9 (see footnote * in Table 3). After examining the values N at this stress ratio, it was found that some of the plain concrete (*0P*) and SFRC specimens (*0BF*) sustained at least 2 million cycles. Conversely, the N values of the SFRRuC specimens (*30BF* and *60BF*) were much lower. Hence, it was decided to use average strength values ($f_{ctm,fl}$) and S of 0.8 and 0.9 for the tests on prisms *0P* and *0BF*, respectively. On the other hand, the flexural fatigue loads for the tests on prisms *30BF* and *60BF* were determined using characteristic values and S of 0.7 and 0.5.

Table 3. Fatigue flexural test results

Mix	Stress ratio, S, based on $f_{ctm,fl}$ ($f_{ctk,fl}$)	Specimen No.	Fatigue life, N	Mix	Stress ratio, S, based on $f_{ctm,fl}$ ($f_{ctk,fl}$)	Specimen No.	Fatigue life, N
0P	0.9 (1.26)	*0P*-1	195	*30BF*	0.78 (0.9*)	*30BF*-1	12,000 +
		0P-2	438			*30BF*-2	217,700 +
		0P-3	482			*30BF*-3	729,700 +
	0.8 (1.12)	*0P*-1	1,200+		0.57 (0.65)	*30BF*-1	2,218
		0P-2	6,968			*30BF*-2	1,690,882
		0P-3	17,800+			*30BF*-3	2,000,000
	0.64 (0.9*)	*0P*-1	733,303		0.43 (0.5)	*30BF*-1	2,000,000
		0P-2	2,000,000			*30BF*-2	2,000,000
		0P-3	2,000,000			*30BF*-3	2,000,000
0BF	0.9 (1.13)	*0BF*-1	431	*60BF*	0.66 (0.9*)	*60BF*-1	3,754
		0BF-2	9,172			*60BF*-2	6,084
		0BF-3	102,718			*60BF*-3	59,690
	0.8 (1.0)	*0BF*-1	16,525		0.51(0.7)	*60BF*-1	58,937
		0BF-2	209,338			*60BF*-2	64,157
		0BF-3	356,807			*60BF*-3	315,080
	0.71 (0.9*)	*0BF*-1	852,009		0.37(0.5)	*60BF*-1	1,600,000
		0BF-2	2,000,000			*60BF*-2	2,000,000
		0BF-3	2,000,000			*60BF*-3	2,000,000

+ Number of cycles recorded in 100 cycle accuracy.
* Initial tests at 0.9$f_{ctk,fl}$

Figure 5 compares the logarithmic number of cycles (log N) endured by each specimen and the relative S calculated using $f_{ctm,fl}$ (quantitative comparisons are included in section 4). It is evident that the fatigue life data have a large scatter even for the same mixes and stress ratios, in particular for specimens with steel fibres and/or rubber particles. Though the uneven distribution of rubber and fibre orientation may significantly contribute to this high variability [1, 20], the fact that specimens from different batches were used also plays a significant role.

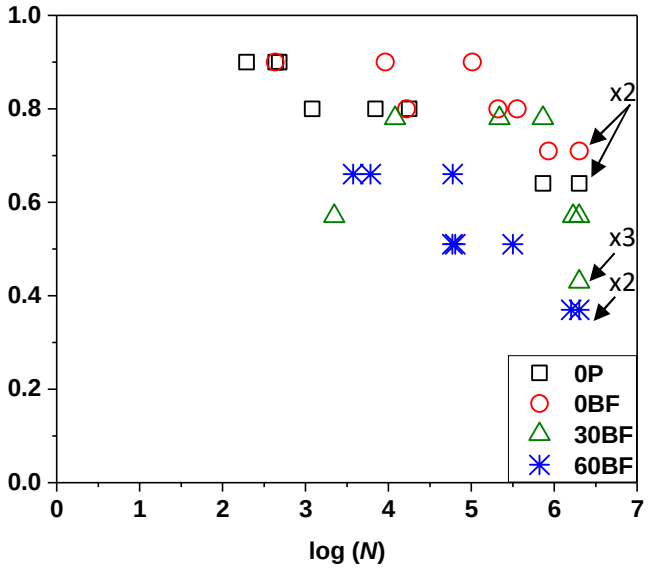

Figure. 5 Test results in terms of logarithmic number of cycles (*log N*) and *S* (based on $f_{ctm,fl}$)

Figure 5 indicates that steel fibre blends improve the performance of specimens *0BF* by increasing its fatigue life. Previous research has proven that RTSF are effective in restraining the propagation of micro-cracks into meso-cracks, whilst MSF are more effective in holding macro-cracks together [1, 38].

The replacement of natural aggregates with rubber in SFRRuC significantly degrades the fatigue performance of specimens *30BF* and *60BF*. This can be attributed to the stiffness and strength degradation in the SFRRuC resulting from the different elastic properties of rubber, as well as to the weak bond between cement paste and rubber. SFRRuC is also highly porous [29], which also contributes to stiffness degradation during cyclic loading.

Figure 6 compares the load-deflection response under static and fatigue load for the examined mixes. The static curve is the average of three prisms, whereas the fatigue curve (one specimen) is representative of typical behaviour observed during the tests. Despite the fact that the applied S (calculated using $f_{ctm,fl}$) is different for all mixes, it is evident that the initial stiffness (slope) of the fatigue loops is similar to that of the static curve. However, the stiffness degrades gradually with the number of fatigue cycles. Note also that the stiffness degrades faster with increasing rubber contents. It is also interesting to note that the *0P* and *0BF* failure occurred when the fatigue cycles touched the monotonic envelope. This may also be the case for *30BF* and *60BF* as one cycle was recorded for every logarithmic step. Though this does not necessarily help to predict fatigue life, but it can give an indication of the likely fatigue behaviour and, most importantly, the maximum displacement at failure.

The damage process in SFRRuC under fatigue loading is expected to progress in three stages: 1) during the first load cycles, flaws and micro-cracks form at the rubber/matrix interface and at the weak region within the concrete; 2) as loading progresses, micro-cracks develop at the rubber/matrix interface and at the fibre/matrix interface, with the former propagating at a faster rate. Although the fibres resist the opening of numerous micro-cracks, these tend to propagate and combine quickly to form macro-cracks; 3) at the final stages of loading (or at failure), a main crack develops after a sufficient number of macro-cracks have formed.

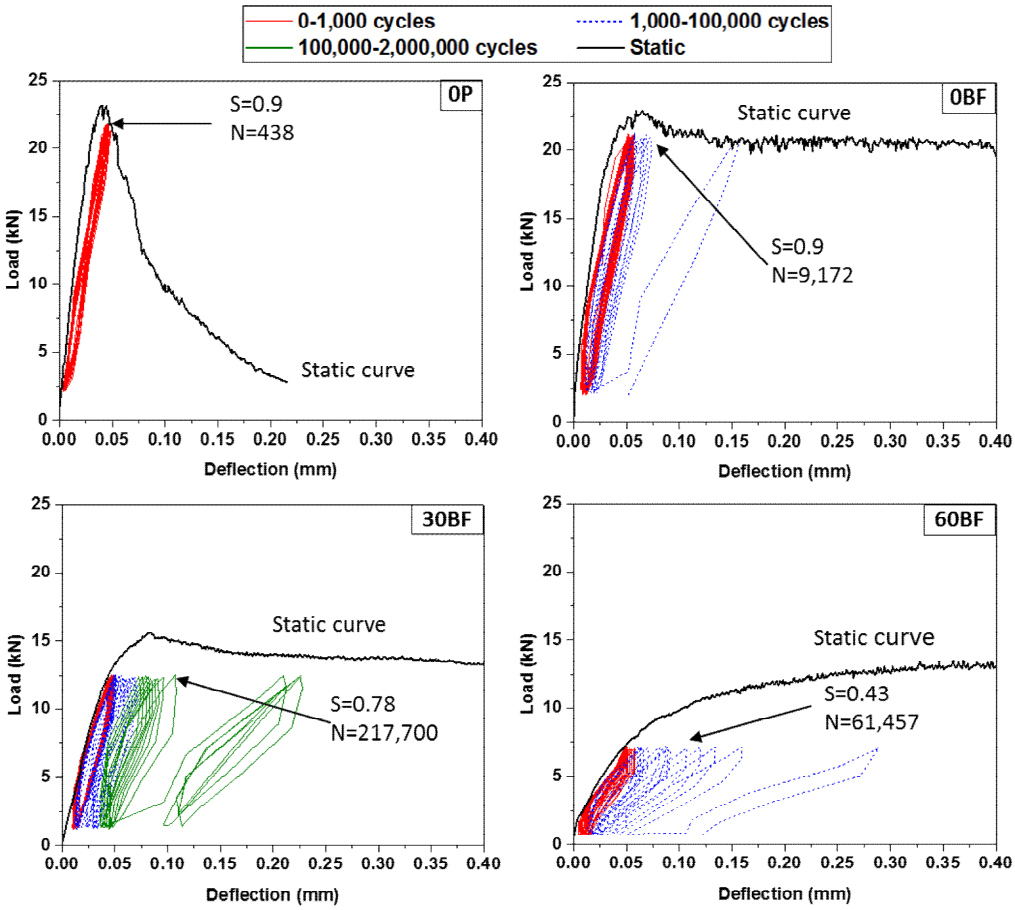

Figure. 6 Load-deflection response under static and fatigue load for examined mixes

The fatigue loops of the SFRRuC (*30BF* and *60BF*) specimens are evidently "fatter" than those of *0P* and *0BF*, thus indicating that the addition of rubber enhances energy dissipation. However, a direct comparison of the energy dissipated by the specimens is not possible due to the different S applied during the tests. Note also that, due to their higher flexibility, SFRRuC specimens exhibit notably higher deflection at failure than that of normal concrete (*0P* and *0BF*). Despite the lower fatigue resistance of SFRRuC mixes with large volumes of rubber, their higher ductility and flexibility can still be used to accommodate subgrade movements of pavement slabs at lower stress levels. To assess the overall fatigue performance of SFRRuC pavement, a probabilistic approach can be adopted, as shown in the following sections.

4 Determination of fatigue-life distribution using probabilistic analysis

In this section, three models: 1) two-parameter Weibull distribution model, 2) graphical interpolation model and 3) the mathematical model are used to derive probabilities of failure (P_f) and *S–N* relationships for each mix, which can be used in pavement design. For comparison purposes, the P_f-*S–N* relationships are compared at probabilities of failure of 25% and 50% (or survival probabilities of 75% and 50%, respectively). These values are widely adopted in the fatigue design of pavements [1, 46-48]. In pavement design, it is usually considered that 2×10^6 cycles correspond to an infinite fatigue life [7, 20, 49] and this assumption is utilised in the following calculations.

4.1 Two-parameters Weibull distribution

The Weibull distribution has been widely used for the statistical analysis of fatigue life data in concrete [7, 36, 49, 50] because it is easy to apply, it is statistically sound and provides accurate results even with a small number of samples, and it has a hazard function that reflects the actual material behaviour in fatigue. The two-parameters of the Weibull distribution (α and u) can be calculated through either i) the graphical method, ii) the method of moments, or iii) the method of maximum-likelihood estimate. In this study, the fatigue life data for each mix and at a given stress ratio S (based on $f_{ctm,fl}$) are analysed, and α and u are estimated using methods i to iii above. The mean values of α and u (average of i to iii) are used to estimate the fatigue lives corresponding to P_f = 0.25 and 0.50, from which the P_f-*S–N* relationships are derived.

4.1.1 Graphical method

The Weibull distribution survival function is defined by [7, 50]:

$$P_s\,(N) = \exp\left[-\left(\frac{N}{u}\right)^{\alpha}\right] \tag{1}$$

where N is the fatigue life, α is the shape parameter (or Weibull slope) at the stress ratio S, and u is the scaling parameter (or characteristic life) at S.

By taking the logarithm twice on both sides of Eq. (1):

$$ln\left[ln\left(\frac{1}{Ps}\right)\right] = \alpha\ln(N) - \alpha\ln(u) \tag{2}$$

If it is assumed that $Y = ln\left[ln\left(\frac{1}{p_s}\right)\right]$, $X = ln(N)$ and $\beta = \alpha ln(u)$, then Eq. (2) can be rewritten as a linear equation:

$$Y = \alpha X - \beta \tag{3}$$

where all the variables are as defined before. Hence, when the fatigue life data at a given stress follow a linear trend (correlation coefficient $r \geq 0.9$), such data are deemed to comply with the Weibull distribution and α and u can be obtained directly from regression analyses [7, 20]. Table 4 summarises the fatigue life data (in ascending order), P_s, X and Y of the tested specimens. In this table, the survival probability P_s is calculated using [49, 50]:

$$P_s = 1 - \frac{i}{K+1} \tag{4}$$

where i is the failure order number, and K is the number of specimens tested at a given stress ratio (K=3 prisms).

Table 4. Analysis of fatigue life data

Mix	S	Fatigue life, N	P_s	X	Y	Graphical method			Method of moments		Maximum likelihood moment		Average		Estimated fatigue life, N_e at P_f of	
						r	α	u	α	u	α	u	α_w	u_w	0.25	0.50
0P	0.9	195	0.75	5.27	-1.25	0.94	1.48	461	2.58	419	3.63	415	2.54	427	262	370
		438	0.50	6.08	-0.37											
		482	0.25	6.18	0.33											
	0.8	1,200	0.75	7.09	-1.25	0.99	0.57	11,208	1.03	8,758	1.13	9,029	0.90	9,569	2,400	6,371
		6,968	0.50	8.85	-0.37											
		17,800	0.25	9.79	0.33											
	0.64	733,303	0.75	13.51	-1.25	0.90	1.22	2,032,791	2.29	1,780,997	3.18	1,771,850	2.21	1,843,261	1,048,809	1,561,514
		2,000,000	0.50	14.51	-0.37											
		2,000,000	0.25	14.51	0.33											
0BF	0.9	431	0.75	6.07	-1.25	1.00	0.29	32,926	0.64	26,868	0.53	22,143	0.48	27,039	2,014	12,594
		9,172	0.50	9.12	-0.37											
		102,718	0.25	11.54	0.33											
	0.8	16,525	0.75	9.71	-1.25	0.96	0.46	272,603	1.15	204,081	1.06	198,163	0.88	222,700	54,233	146,979
		209,338	0.50	12.25	-0.37											
		356,807	0.25	12.78	0.33											
	0.71	852,009	0.75	13.66	-1.25	0.90	1.44	2,028,617	2.62	1,820,457	3.74	1,804,209	2.57	1,865,583	1,149,396	1,617,843
		2,000,000	0.50	14.51	-0.37											
		2,000,000	0.25	14.51	0.33											
30BF	0.78	12,000	0.75	9.39	-1.25	0.99	0.37	396,881	0.86	295,090	0.76	278,790	0.66	320,351	47,821	183,078
		217,700	0.50	12.29	-0.37											
		729,700	0.25	13.50	0.33											
	0.57	2,218	0.75	7.70	-1.25	0.91	0.18	1,999,505	1.16	1,295,849	0.47	818,064	0.60	1,357,428	169,741	736,371
		1,690,882	0.50	14.34	-0.37											
		2,000,000	0.25	14.51	0.33											
	0.43	2,000,000	0.75	14.51	-1.25	0.00^+	0.00^+	0.00^+	0.00^+	0.00^+	0.00^+	0.00^+	0.00^+	0.00^+	2,000,000	2,000,000
		2,000,000	0.50	14.51	-0.37											
		2,000,000	0.25	14.51	0.33											
60BF	0.66	3,754	0.75	8.23	-1.25	0.91	0.49	26,817	0.71	18,660	0.84	20,913	0.67	21,909	3,434	12,701
		6,084	0.50	8.71	-0.37											
		59,690	0.25	11.00	0.33											
	0.51	58,937	0.75	10.98	-1.25	0.85^*	0.71	193,571	1.00	145,901	1.29	159,403	0.99	164,629	46,870	113,763
		64,157	0.50	11.07	-0.37											
		315,080	0.25	12.66	0.33											
	0.37	1,600,000	0.75	14.29	-1.25	0.90	5.49	2,007,453	9.55	1,965,979	14.25	1,946,702	9.67	1,953,644	1,717,428	1,880,968
		2,000,000	0.50	14.51	-0.37											
		2,000,000	0.25	14.51	0.33											

$^+$ All of three specimens recorded 2M fatigue cycles, therefore, all point in the curve are aligned. * Correlation coefficient less than 0.9.

Figure 7 plots the values X and Y for mix *0BF*. The results show that the fatigue life data for the same stress ratio follow a linear trend. This confirms that α represents the slope of the curve, while u can be calculated using the curve intercept point. Similar trends were observed for the rest of the data, and the results of α and u obtained from the graphical method are listed in Table 4. It is shown that in most cases $r \geq 0.9$, thus indicating that a linear relationship exists between X and Y. Since all the three prisms *30BF* at S=0.43 reached 2×10^6 fatigue cycles, the three points in the graph are aligned vertically, thus leading to a zero slope (i.e. α=0). Although r=0.85 for *60BF* at S=0.51, the probabilistic analysis is still carried out and the results are subsequently adjusted using the average values of the Weibull distribution parameters, as explained later.

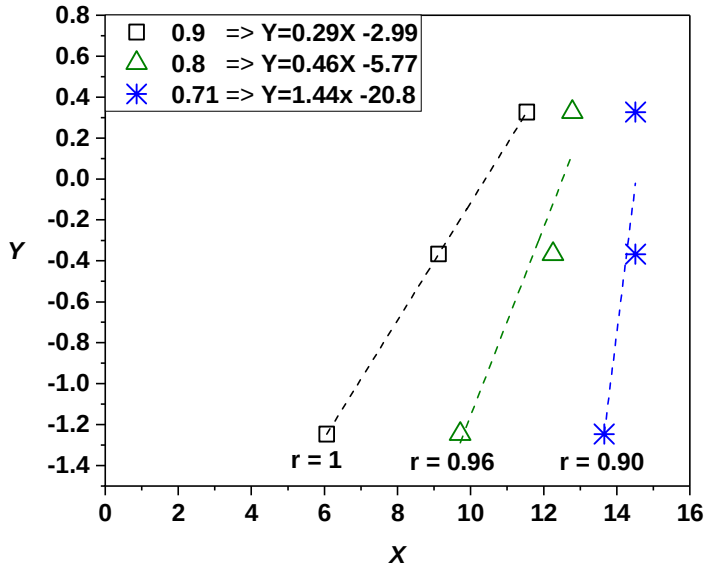

Figure. 7 Graphical analysis of fatigue-life data for *0BF*

4.1.2 Method of moments

This method calculates α and u at each stress ratio using the mean fatigue life (μ) of three prisms, and the corresponding coefficient of variation (CV) according to the following equations [36, 49-51]:

$$\alpha = (CV)^{-1.08} \tag{5}$$

and

$$u = \frac{\mu}{\Gamma\left(\frac{1}{\alpha}+1\right)} \tag{6}$$

where $\Gamma(\ )$ is the gamma function.

Table 4 summarises the values α and u for all concrete mixes at various stress ratios using the method of moments.

4.1.3 Method of maximum-likelihood estimate

The probability density function of the Weibull distribution can be written as [36, 50, 51]:

$$f_N(N) = \frac{\alpha}{\theta} N^{\alpha-1} \exp\left[\frac{N^{\alpha}}{\theta}\right] \tag{7}$$

where

$$\theta = u^{\alpha} \tag{8}$$

The maximum-likelihood function can be expressed as follows [36, 50, 51]:

$$\frac{\sum_{i=1}^{K} N_i^{\alpha^*} \ln(N_i)}{\sum_{i=1}^{K} N_i^{\alpha*}} - \frac{1}{\alpha^*} = \frac{1}{K} \sum_{i=1}^{K} \ln(N_i) \tag{9}$$

$$\theta^* = \frac{1}{K} \sum_{i=1}^{K} N_i^{\alpha^*} \tag{10}$$

where α^* and θ^* are the maximum-likelihood estimators for α and θ, respectively, and the rest of the variables are as defined before. Accordingly, the value α^* is first obtained iteratively using Eq. (9), and then replaced in Eq. (10) to calculate θ^*. The parameter u is finally calculated using α^* and θ^* (instead of α and θ) in Eq (8). Table 4 summarises the values α and u for all concrete mixes at various stress ratios using the method of maximum-likelihood estimate.

The results in Table 4 show that the three methods lead to significantly different values of α and u, with the graphical method yielding α and u values considerably different from those obtained by the other two methods. This is due to the small number of prisms (three) tested at each stress ratio, as well as to the large scatter in the fatigue life data. To address this issue and adopt a more conservative approach, the average values of α and u of the three methods are considered. The average values are shown as α_w and u_w in Table 4.

4.1.4 *Ps-S-N* relationships

The values α_w and u_w of the Weibull distribution parameters (Table 4) are used here to estimate the fatigue lives corresponding to P_f = 0.25 and 0.50 (P_s=0.75 and 0.50). The fatigue life N_e at certain S and P_f can be estimated using a rearranged version of Eq. (2) [36]:

$$N_e = ln^{-1}\left[\frac{ln\left[ln\left(\frac{1}{1-P_f}\right)\right] + \alpha_w \ln(u_w)}{\alpha_w}\right] \tag{11}$$

Table 4 compares the values N_e calculated using Eq. (11) at P_f = 0.25 and 0.50. The results show that, as expected, for the same stress ratio the value N_e increases with the probability of failure. Additionally, for the same probability of failure, N_e increases as the stress ratio decreases.

Using the estimated fatigue lives N_e in Table 4, the P_f-*S*-*N* relationships can be derived using the double logarithmic fatigue equation, which has been used in previous studies [7, 19]:

$$\log(S) = a + b\log(N_e) \tag{12}$$

Figure 8 shows the calculated P_f-*S*-*N* relationships for all concrete mixes using N_e values at P_f=0.25 and 0.50. The constants a and b in Eq. (12) are obtained from regression analyses of the data shown in Figure 8. It is shown that r is always close to 1 for all concrete mixes at both probability of failures, which confirms the linear trend of the test data. Note that the equations in Figure 8 can be used to calculate the stress ratio for a known fatigue life at P_f=0.25 and 0.50, as shown in section 4.4.

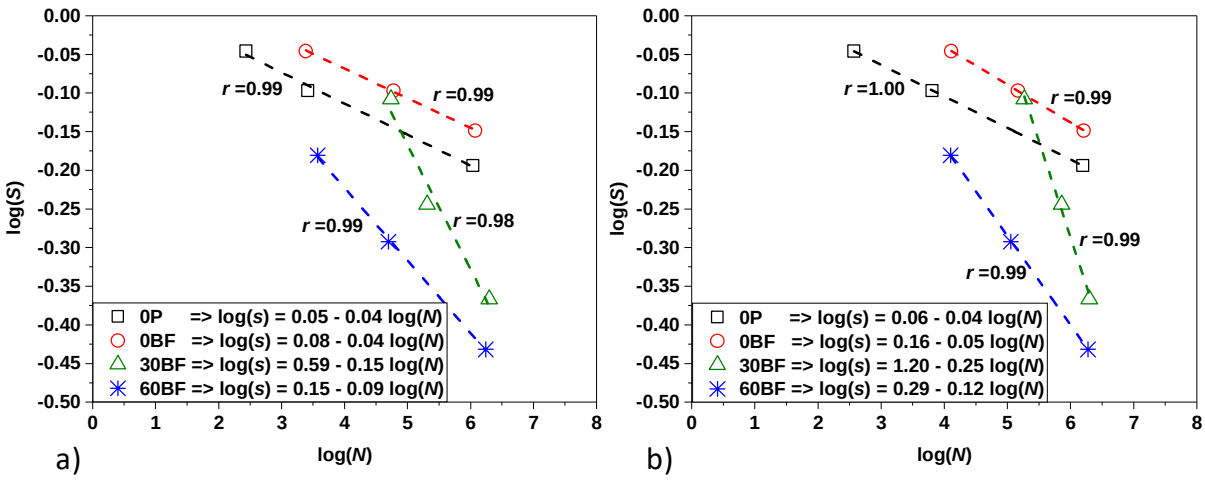

Figure. 8 Fatigue curves of all concrete mixes corresponding to a) P_f = 0.25 and b) P_f = 0.50

4.2 Graphical interpolations

The graphical interpolation model is suitable for practical design because it presents concisely the P_f-*S*-*N* relationships, and it is fast and computationally simple. To generate the P_f-*S*-*N* relationships, the specimens are initially sorted in ascending order of fatigue life [44, 52, 53]. The probability of failure is defined as $\frac{j}{n+1}$, where j is the rank of the specimen and n is the number of specimens tested for each mix at a particular stress ratio. Table 5 shows the specimens of mix *0BF* ranked according to their fatigue life, as well as the calculated P_f values.

Table 5. Ranked specimens in terms of N according to stress ratio for mix *0BF*.

j	Fatigue life, N, at stress ratio of (based on $f_{ctm,fl}$)			$P_f = \frac{j}{(n+1)}$
	0.9	0.8	0.71	
1	431	16,525	852,009	0.25
2	9,172	209,338	2,000,000	0.50
3	102,718	356,807	2,000,000	0.75

The P_f-S-N relationships for mix *0BF* are shown in Figures 9a-c. In this method, a P_f-N curve is initially plotted for each stress ratio using P_f and log(N), as shown in Figure 9a for the data in Table 5. Based on linear regressions, the S-N curves are then derived using the stress ratios S (based on $f_{ctm,fl}$) and log(N) for each P_f, as shown in Figure 9b. The S-P_f curves in Figure 9c are finally obtained by graphical interpolation for different fatigue lives. For instance, for a fatigue life N=500,000 cycles (log (N)=5.7), the estimated stress ratio is S_e=0.76 (see Figure 9b) for P_f=0.50. Alternatively, the linear equations obtained by regression analyses in the S-N curves (see Figure 9b) can be used to estimate the stress ratio. Different N can be selected in the last step for comparison. In this study, N=500,000, 1,000,000 and 2,000,000 cycles are adopted. The P_f-S and S-N curves for mixes *0P*, *30BF* and *60BF* calculated following the above procedure are shown in Figure 10. Further comparisons of the results shown in Figures 9 and 10 are included in section 4.4.

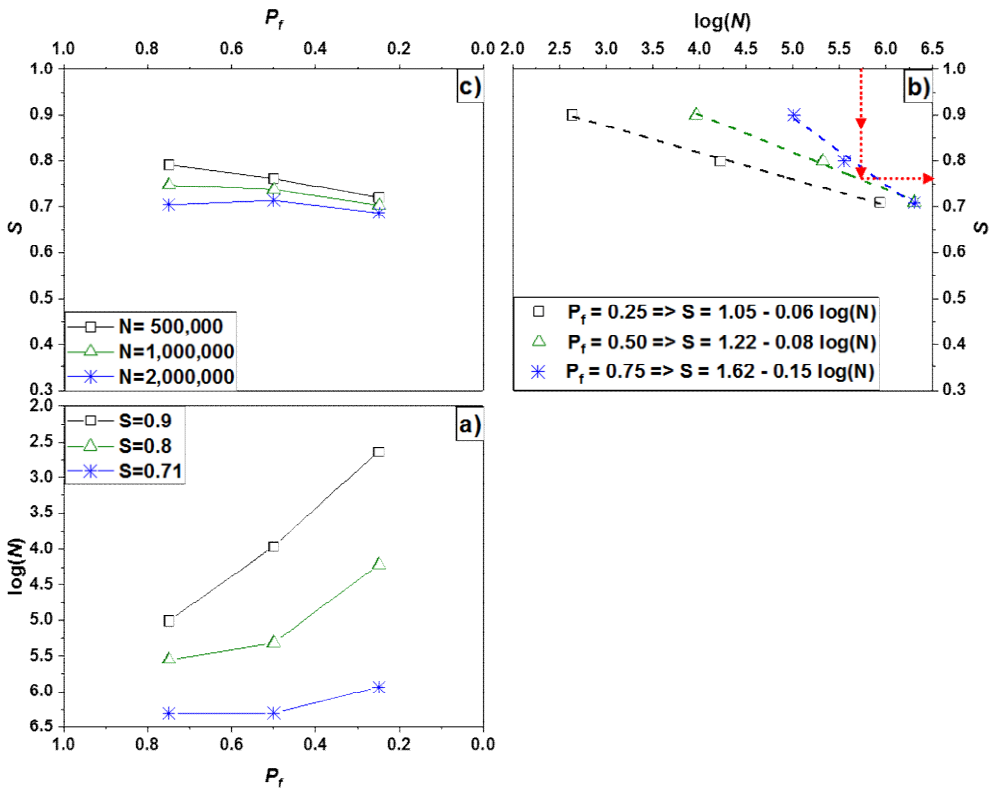

Figure. 9 Graphical interpolation example for mix *0BF* a) P_f-N, b) N-S and c) P_f-S curves

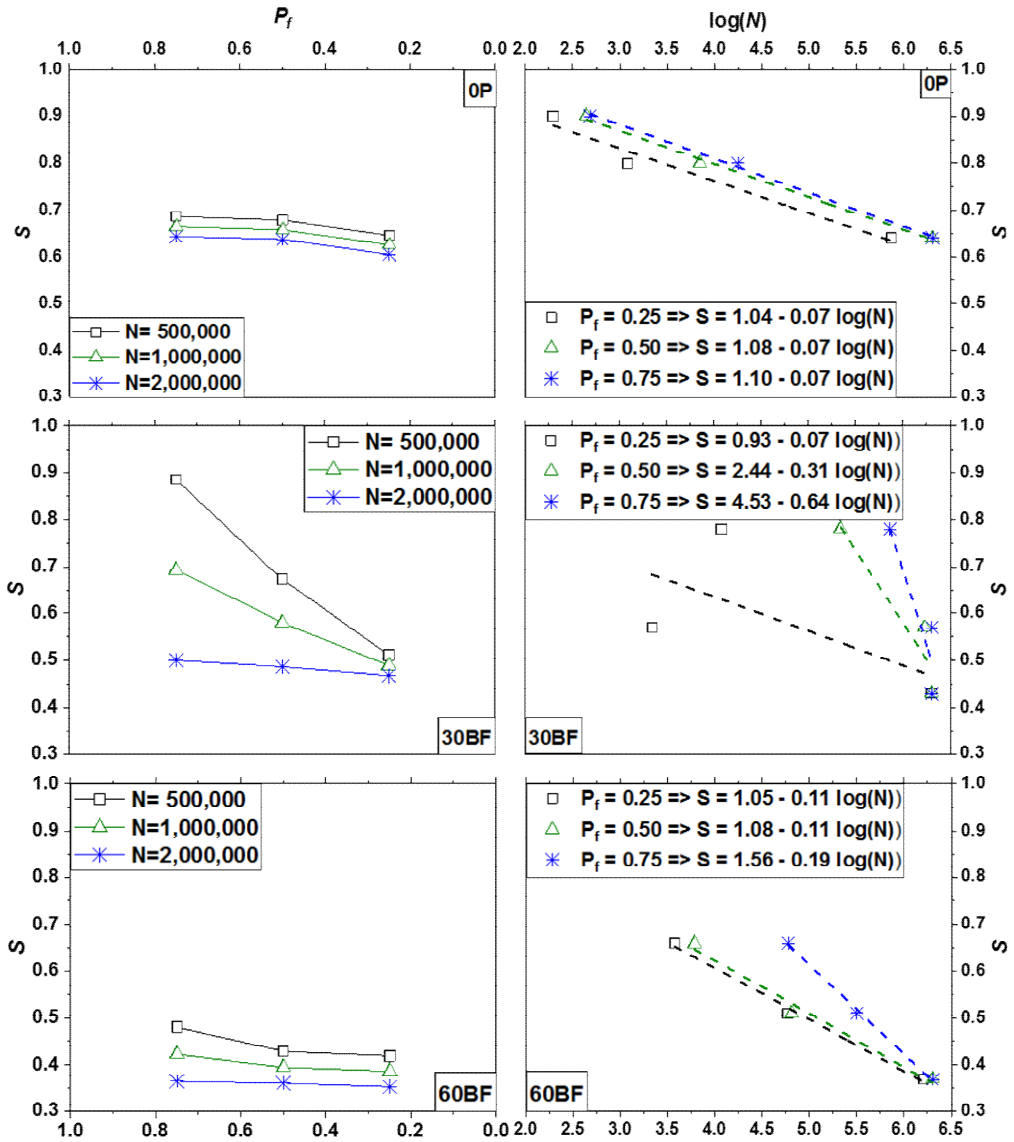

Figure. 10 Graphical interpolation results for mixes *0P*, *30BF* and *60BF*: *S*-P_f and *S*-*N* curves

4.3 Mathematical models

Previous research has proposed a mathematical function to derive P_f-*S*-*N* relationships for SFRC [1, 44, 52]. The mathematical function can be expressed as:

$$P_f = 1 - 10^{-a\, S^b\, (log\, N)^c} \tag{13}$$

where *a*, *b* and *c* are experimental coefficients derived from statistical analyses of the fatigue life data, as described in references [44, 52, 53]. The coefficient *a*, *b* and *c* obtained for the mixes examined in this study are summarised in Table 6. Such coefficients can be replaced in Eq. (13) to estimate the stress ratio S_e for any values of N and P_f.

Table 6. Experimental coefficients *a*, *b* and *c* calculated from the mathematical model.

Mix	Experimental coefficients		
	a	*b*	*c*
0P	8.77E-04	21.50	8.39
0BF	1.43E-03	10.07	4.76
30BF	2.91E-04	1.71	4.62
60BF	2.27E-06	8.35	10.87

4.4 Comparison between models

Table 7 compares the estimated fatigue stress ratio S_e for a fatigue life of 2×10^6 cycles and P_f=25% and 50% obtained from the probabilistic models described in sections 4.1, 4.2 and 4.3. With the exception of *30BF*, the estimated fatigue stress ratios obtained from the three models agree well for all mixes at the same P_f. The low stress ratios given by the mathematical model for *30BF* can be attributed to the fact that the three specimens for S=0.43 reached 2×10^6 fatigue cycles (see Table 3), which leads to a very low coefficient *b* (see Table 6). The average stress ratio of the three models can be used for practical pavement design, as demonstrated by an example in the following section.

Table 7. Summary of the fatigue stress ratio obtained from three methods.

Mix	P_f	Estimated S_e based on			Average stress ratio, $S_{e,ave}$
		Weibull distribution	Graphical interpolation	Mathematical	
0P	25%	0.62	0.60	0.61	0.61
	50%	0.63	0.64	0.64	0.64
0BF	25%	0.70	0.69	0.65	0.68
	50%	0.70	0.71	0.71	0.71
30BF	25%	0.42	0.47	0.24	0.45^+
	50%	0.44	0.49	0.40	0.47^+
60BF	25%	0.36	0.35	0.34	0.35
	50%	0.37	0.36	0.37	0.37

$^+$ Value calculated based on the Weibull distribution and graphical methods only.

5 Design implications

To assess the effect of the addition of steel fibres and/or rubber on the thickness *h* of rigid pavement slabs, a road section with a standard axle load *W* is assumed. According to Westergaard's empirical-theoretical model [54], the rigid pavement can be modelled as a thin elastic plate on a soil subgrade. The stress at the edge (critical location) is:

$$\sigma_{max} = \frac{0.572\,W}{h^2}\left[4\log\left(\frac{I}{\sqrt{1.6\,Z^2 + h^2} - 0.675\,h}\right) + 0.359\right] \quad (14)$$

where σ_{max} is the maximum tensile stress of the slab modified to account for fatigue by multiplying the flexural strength ($f_{ctm,fl}$ listed in Table 2) by the average fatigue stress ratio $S_{e.ave}$ at P_f=25% (i.e. values from last column in Table 7); Z is an equivalent contact radius of the tyre; and I is the radius of the relative stiffness of the slab, defined by:

$$I = \sqrt[4]{\frac{E_s\ h^3}{12\ (1 - \nu^2)\ M_k}} \quad (15)$$

where ν is the Poisson's ratio of the slab material; M_k is the modulus of elastic subgrade reaction; and E_s is shown in Table 2. In this study, M_k is the modulus of resilience of the soil and measures the ability of the ground to resist immediate elastic deformation under load.

The slab thickness h for all concrete mixes was calculated using the modified Westergaard's method and the following (typical) values: W=80 kN, M_k=80 MPa/m, and Z=190 mm (assuming a tyre pressure of 7 bar), and ν=0.2. The subgrade is taken to be a very well consolidated made of gravels and sandy gravels [55]. Although mixes *0P* and *0BF* have similar average static flexural strength and elastic modulus, the addition of fibres reduces the slab thickness by 7% (h=173 mm for *0P* vs h=161 mm for *0BF*). This is mainly due to the enhanced fatigue performance resulting from the addition of fibres, as discussed in section 3.3. On the other hand, the replacement of natural aggregates with rubber particles increases the slab thickness to 256 mm and 305 mm for mixes *30BF* and *60BF*, respectively. This is due to the reduced mechanical and fatigue properties of SFRRuC mixes (sections 3.2 and 3.3), which leads to a low radius of relative stiffness I (Eq. (15)).

Based on these results, it is evident that the modified Westergaard's method does not show the expected benefits of using steel fibres and/or rubber over plain concrete. This is because the method was originally developed for plain concrete, which behaves in a linear elastic manner up to tensile failure. As such, the effect of deformability (i.e. ductility and flexibility) which will help to accommodate subgrade movements are not accounted for in the equations. To assess the deformability of SFRRuC, the authors performed three-point bending tests on notched prisms according to RILEM [45], and the stress versus crack mouth opening displacement (CMOD) curves are shown in Figure 11. The enhancement in flexibility is demonstrated by progressively larger CMODs at maximum stress with increasing rubber content, resulting from the ability of rubber to reduce stress concentration at the crack tip and to delay micro-crack propagation [24]. Likewise, the post-peak behaviour is also improved by

the inclusion of fibres, and it is further enhanced by the rubber. For example, at a stress level of 3MPa, mixes *30BF* and *60BF* have larger CMODs than that of 0*BF*, thus confirming the enhancement in ductility as discussed in section 3.1. Hence, in order to identify the benefits of using steel fibres and/or rubber in concrete, it is necessary to use design equations that take into account the flexibility and ductility that SFRRuC can offer.

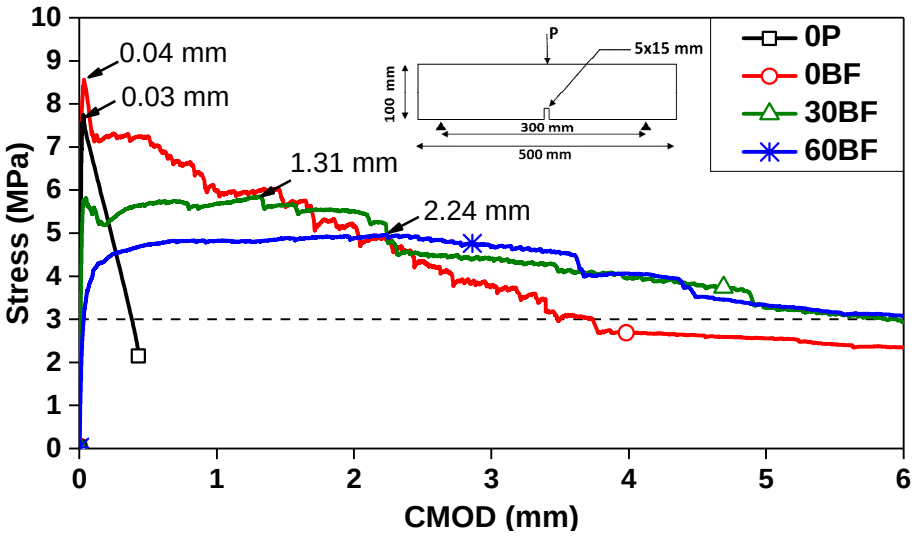

Figure. 11 Average stress-CMOD curves for prisms

The Technical Report 34 (TR34) by the Concrete Society [56] can be used to show the advantages of using SFRRuC pavements. TR34 designs SFRC slabs at the ultimate limit state (ULS) using the yield line theory. Accordingly, the flexural moment at the bottom of the slab and along the sagging yield lines (M_p) are considered to be fully plastic (i.e. residual post-cracking behaviour exist), as shown in Eq. (16). At the same time, cracks must be avoided at the top surface of the slab and the moment capacity along the hogging yield lines (M_n), as shown in Eq. (17), should be always greater than the ultimate design moment of the concrete.

$$M_P = \frac{h^2}{1.5}\,(0.29\,\sigma_4 + 0.16\,\sigma_1) \tag{16}$$

$$M_n = \frac{f_{ctm,fl}}{1.5}\left(\frac{h^2}{6}\right) \tag{17}$$

where $\sigma_1 = 0.45 \cdot CMOD_1$, and $\sigma_4 = 0.37 \cdot CMOD_4$. In this study, values of $CMOD_1$=0.5 mm and $CMOD_4$=3.5 mm (as obtained from three-point bending tests on notched prisms [45]) are used to calculate σ_1 and σ_4. The slab thickness h can be calculated using Eq. (18) [56] for a free edge load.

$$W = \frac{[\pi\,(M_P + M_n) + 4\,M_n]}{\left[1 - \left(\frac{2\,Z}{3\,I}\right)\right]} \quad (18)$$

The design approach adopted by TR34 neglects the effect of fatigue load. To address this drawback and account for fatigue, it is thus proposed to modify this approach and multiply $\boldsymbol{f}_{ctm,fl}$ in Eq. (17) by $S_{e.ave}$ (section 4.4).

Figure 12 compares the slab thickness calculated using the modified TR34 approach and modified Westergaard's method. It is shown that the adoption of the proposed modified TR34 approach reduces the slab thickness calculated by the modified Westergaard's method by 20% for *0P*, 32% for *0BF*, 44% for *30BF* and 50% *60BF* mixes. These results confirm the benefits of using steel fibres and/or rubber in concrete. It is also shown that, although the fatigue strength of SFRRuC is relatively low, the thickness of slabs produced with this novel material is similar to that of slabs built with plain concrete. However, unlike plain concrete pavements, SFRRuC pavements represent a potential solution to accommodate subgrade movements during service life. Consequently, it is recommended to use the proposed modified TR34 approach for the design of flexible SFRRuC pavements.

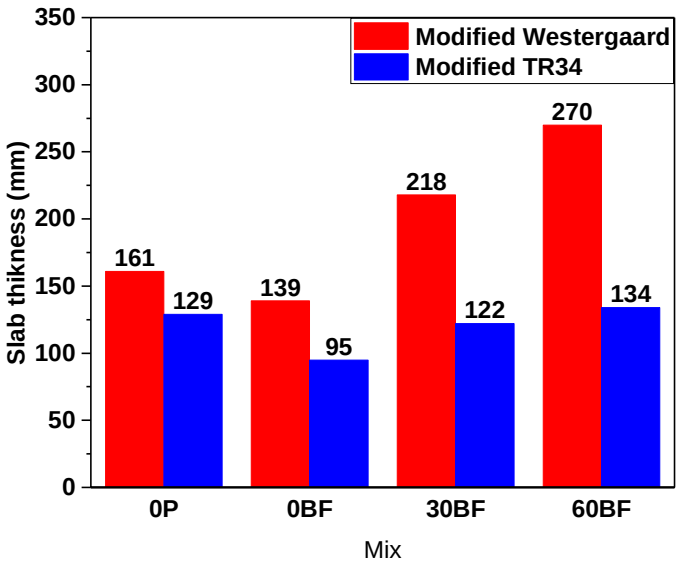

Figure. 12 Slab thickness comparison for all concrete mixes

The capability of flexible SFRRuC pavements to accommodate subgrade settlements is demonstrated through finite element (FE) analysis in the following section.

6 Finite Element Modelling

A two-dimensional (2D) plane strain model of a pavement slab was developed in the FE software ABAQUS® [57]. Recent research [58] has shown that 2D plane strain models provide similar results to 3D models (differences of less than 2%) in the study of transverse profiles of pavements with large longitudinal dimensions. To show the true benefits of flexible SFRRuC, two pavements designed using the modified TR34 approach (Figure 12) were modelled: i) a SFRC pavement (*0BF*) of 95 mm depth; ii) a SFRRuC pavement (*60BF*) of 134 mm depth. The pavements were assumed to be on top of a stiff clay subgrade of length=10.0 m and depth=4.0 m, as shown in Figure 13a. The length of the pavement was chosen to prevent boundary and edge effects. Previous research has shown that there are no subgrade deformations beyond such depth [59]. Two scenarios were considered: 1) a continuous subgrade (Figure 13b), and 2) a subgrade with a gap filled with loose material (length=1 m, depth=0.10 m, see Figure 13c). The gap is intended to simulate common defects arising from non-uniform subgrades due to deterioration developing over time, such as settlement due to poor compaction during construction or temperature variations and freeze-thaw.

8-node quadrilateral plane strain reduced integration elements (CPE8R) were used for the analyses. An initial convergence analysis was performed to optimise the characteristics of the mesh. Based on these results, only a fine mesh was selected for the loading area. The total number of nodes and elements was 14962 and 4800, respectively.

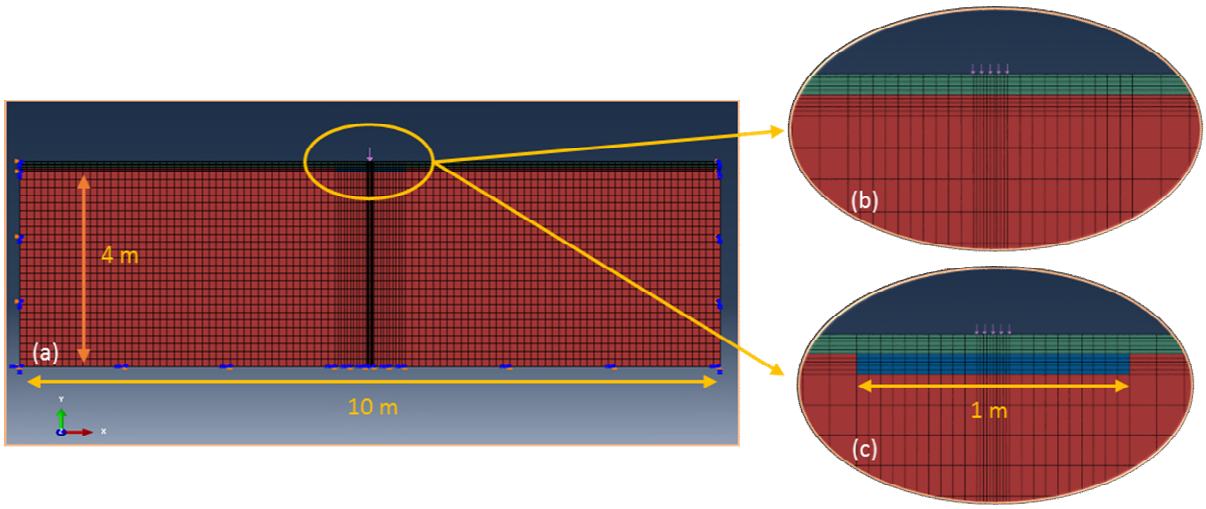

Figure. 13 Finite element model: a) discretised pavement and subgrade, b) continuous subgrade, c) subgrade with a gap

The bottom edge of the subgrade was fixed to prevent horizontal and vertical movements. The boundary nodes along the pavement edges were constrained horizontally only. A Coulomb friction law was used to define the surface-to-surface contact interaction between the pavement

and subgrade (friction parameter=0.3). The load (standard axle) on the pavement was applied through a static contact pressure of 800 kPa. Previous research has widely adopted the Mohr-Coulomb plasticity criterion for subgrade analysis [60], hence, this criterion is used to model the inelastic behaviour of the subgrade and the filling material in the gap. Table 8 summarises the soil properties used in the FE analyses.

Table 8. Assumed soil properties used in FE analyses.

Soil	Elastic modulus (MPa)	Poisson's ratio, ν	Friction angle, φ (º)	Dilation angle ψ (º)	Yield stress (KPa)	Plastic strain
Stiff Clay (subgrade)	80	0.45	0	0	200	0
Loose Sand (hole filling)	10	0.20	28	0	1	0

The concrete was modelled using the concrete damaged plasticity (CDP) constitutive model built-in in ABAQUS®. This model accounts for the inelastic behaviour of concrete in both tension and compression, and can include damage. The model considers two main failure mechanisms in concrete: tensile cracking and compressive crushing. The stress-strain relationship for uniaxial concrete in tension was obtained using inverse analysis [61, 62]) on the load-deflection curves presented in Figure 6b and d. The values for the CDP model (dilation angel=30, eccentricity=0.1, $\frac{F_{b0}}{f_{c0}}$ =1.116, K=0.667 and viscosity=1×10^{-5}) were taken from previous research [61, 63, 64] using SFRC.

Figure 14 compares the plastic strain distribution (cracks) for the SFRC pavement (*0BF*) considering the two scenarios. Whilst wide localised cracks develop in both scenarios, the results in Figure 14b indicate that cracks can be up to 5 times wider if a gap develops under the pavement. It is also shown that if the pavement settles, two wide cracks propagate through the pavement towards its top surface within the loaded area. This implies that the pavement would experience significant damage due to multiple wide cracks, thus jeopardising its serviceability requirements.

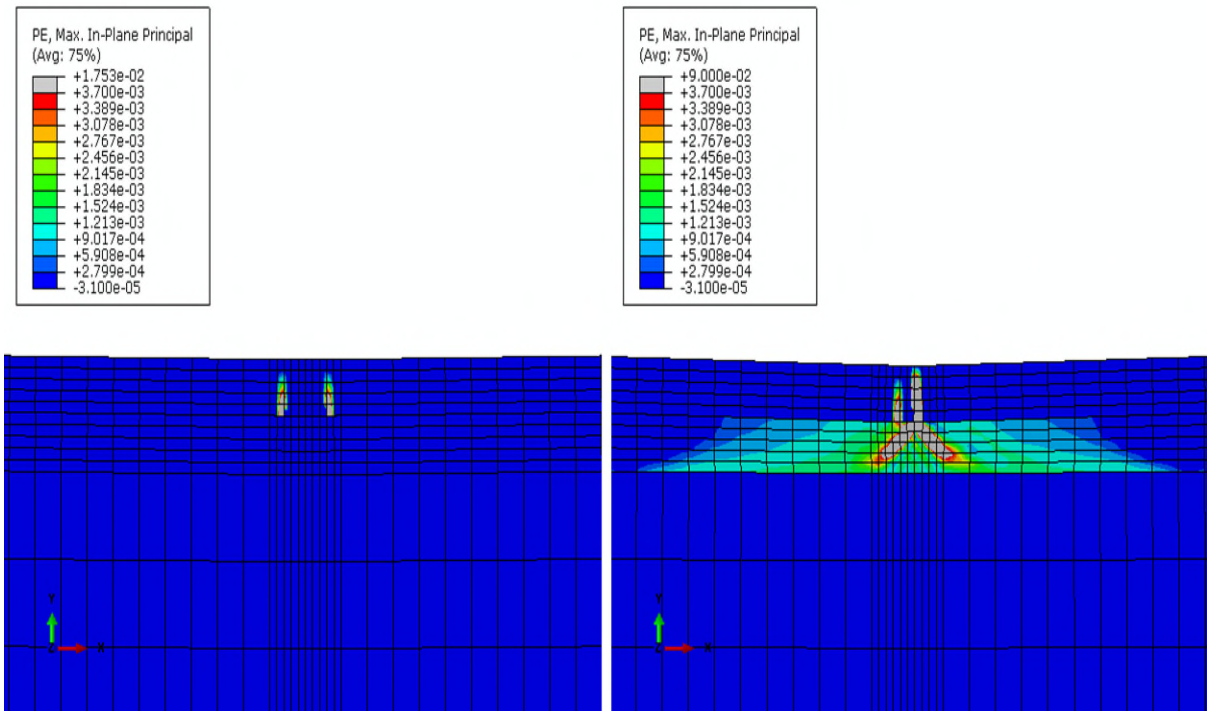

Figure. 14 Plastic strain model *0BF*-95 mm a) without a gap, and b) with 10 cm ×1 m gap.

Figure 15 compares the plastic strain distribution (cracks) for the SFRRuC pavement (*60BF*) considering both scenarios. Figure 15a shows that some minor cracks develop in the pavement on the continuous subgrade. However, these cracks are more spread and up to 7 times narrower compared to the SFRC pavement (see Figure 14a). In presence of the gap (Figure 15b), the cracks in the SFRRuC pavement are not only more evenly distributed over a larger area, but also significantly narrower (up to 24 times) than those in the SFRC pavement. Even when the same depth of 134 mm is used for the SFRC pavement, the cracks are still 10 times larger than the SFRRuC pavement. This shows that flexible SFRRuC pavements are capable of accommodating subgrade movements and settlements more effectively than their SFRC counterparts.

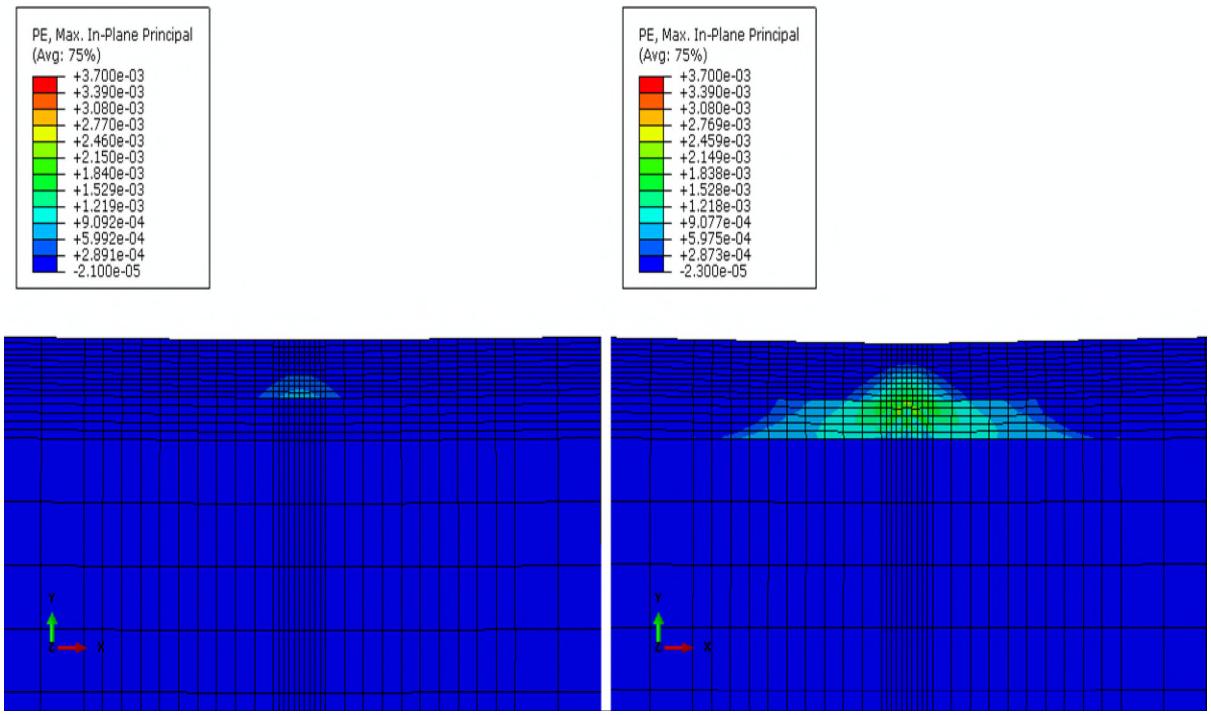

Figure. 15 Plastic strain for model *60BF*-134 mm a) without a gap, and b) with 10 cm ×1 m gap.

It should be mentioned that previous research by the authors showed that optimised flexible SFRRuC a) is highly ductile and flexible [8], and b) that such concrete meets the flexural strengths specifications defined in pavement design [28] . The authors have also demonstrated the adequate durability and long term performance of SFRRuC [29, 30]. In this article, the authors prove that (despite its lower fatigue resistance) SFRRuC can accommodate large subgrade movements and settlements. The experimental, analytical and numerical evidence confirm that SFRRuC is a promising solution for building sustainable road pavements, particularly considering that reusing end-of-life tyre materials (WTR and RTSF) in concrete can contribute to reducing stockpiles of discarded tyres. It should be also noted that, due to the limited number of specimens and mixes examined in the above studies, further research is necessary to fully understand the mechanical behaviour and long-term performance of different SFRRuC mixes with other mix proportions and tested with different stress ratios (e.g. 6 specimens tested at each stress level). Current research by the authors is validating the predictions given by the modified TR34 approach against additional experiments so as to provide practical design guidelines.

7 Conclusions

This study assesses the mechanical and fatigue performance of steel fibre reinforced rubberised concrete (SFRRuC) using fatigue flexural loads on prisms. Based on the results in this study, the following conclusions are drawn:

- A blend of steel fibres in concrete enhances its compressive strength by 20%, while the flexural strength and elastic modulus remain roughly the same. The addition of rubber as aggregate decreases significantly the compressive strength, static flexural strength and elastic modulus of SFRRuC. However, the combination of fibres and rubber enhances the tensile capacity of SFRRuC.
- The relationships between probability of failure, stress ratio and fatigue life (P_f-S–N) given by three probabilistic models widely used in pavement design agree reasonably well. They also provide comparable estimates of fatigue stress ratios that can be used for the practical design of SFRRuC pavements.
- The modified Westergaard's approach does not show the benefits of adding blends of steel fibres or rubber to concrete since the post-peak behaviour of concrete is neglected. The use of the modified TR34 design approach proposed in this study leads to thinner slab thickness when compared to the modified Westergaard's model. Consequently, it is recommended to use this approach for the design of SFRRuC flexible pavements.
- FE analyses indicate that flexible SFRRuC pavements can accommodate large subgrade settlements, thus making such pavements an attractive solution for road pavement applications.

Acknowledgements

The authors would also like to thank all of the material suppliers and companies for their in-kind contribution of materials for this research study: Tarmac UK, Sika, Aggregate Industries UK Ltd, Twintech, and Twincon Ltd.

Disclosure

Funding: This study was funded by the European Union Seventh Framework Programme [FP7/2007–2013] under grant agreement no 603722.

References

[1] A.G. Graeff, K. Pilakoutas, K. Neocleous, and M.V.N. Peres, *Fatigue resistance and cracking mechanism of concrete pavements reinforced with recycled steel fibres recovered from post-consumer tyres*, Engineering Structures 45 (2012) 385-395.

[2] P.C. Perdikaris, A.M. Calomino, and A. Chudnovsky, *Effect of fatigue on fracture toughness of concrete*, Journal of engineering mechanics 112 (8) (1986) 776-791.

[3] M. Lee and B. Barr, *An overview of the fatigue behaviour of plain and fibre reinforced concrete*, Cement and Concrete Composites 26 (4) (2004) 299-305.

[4] O.A. Abaza and Z.S. Hussein, *Flexural Behavior of Steel Fiber-Reinforced Rubberized Concrete*, Journal Of Materials In Civil Engineering 28 (1) (2015) 04015076.

[5] T. Nguyen, A. Toumi, and A. Turatsinze, *Mechanical properties of steel fibre reinforced and rubberised cement-based mortars*, Materials & Design 31 (1) (2010) 641-647.

[6] A. Grinys, H. Sivilevičius, D. Pupeikis, and E. Ivanauskas, *Fracture of concrete containing crumb rubber*, Journal of Civil Engineering and Management 19 (3) (2013) 447-455.

[7] F. Liu, W. Zheng, L. Li, W. Feng, and G. Ning, *Mechanical and fatigue performance of rubber concrete*, Construction and Building Materials 47 (2013) 711-719.

[8] A. Alsaif, L. Koutas, S.A. Bernal, M. Guadagnini, and K. Pilakoutas, *Mechanical performance of steel fibre reinforced rubberised concrete for flexible concrete pavements*, Construction and Building Materials 172 (2018) 533-543.

[9] S. Raffoul, R. Garcia, D. Escolano-Margarit, M. Guadagnini, I. Hajirasouliha, and K. Pilakoutas, *Behaviour of unconfined and FRP-confined rubberised concrete in axial compression*, Construction and Building Materials 147 (2017) 388-397.

[10] F. Hernández-Olivares, G. Barluenga, M. Bollati, and B. Witoszek, *Static and dynamic behaviour of recycled tyre rubber-filled concrete*, Cement And Concrete Research 32 (10) (2002) 1587-1596.

[11] S. Raffoul, R. Garcia, K. Pilakoutas, M. Guadagnini, and N.F. Medina, *Optimisation of rubberised concrete with high rubber content: An experimental investigation*, Construction and Building Materials 124 (2016) 391-404.

[12] R. Siddique and T.R. Naik, *Properties of concrete containing scrap-tire rubber–an overview*, Waste management 24 (6) (2004) 563-569.

[13] Z. Khatib and F. Bayomy, *Rubberized portland cement concrete*, Journal Of Materials In Civil Engineering 11 (3) (1999) 206-213.

[14] A. El-Dieb, M. Abd El-Wahab, and M. Abdel-Hameed, *Mechanical, Fracture, and Microstructural Investigations of Rubber Concrete*, Journal Of Materials In Civil Engineering (10) (2008) 640-649.

[15] A.R. Khaloo, M. Dehestani, and P. Rahmatabadi, *Mechanical properties of concrete containing a high volume of tire–rubber particles*, Waste management 28 (12) (2008) 2472-2482.

[16] E. Ganjian, M. Khorami, and A.A. Maghsoudi, *Scrap-tyre-rubber replacement for aggregate and filler in concrete*, Construction and Building Materials 23 (5) (2009) 1828-1836.

[17] M.A. Aiello and F. Leuzzi, *Waste tyre rubberized concrete: properties at fresh and hardened state*, Waste Manag 30 (8-9) (2010) 1696-704.

[18] C. Wang, Y. Zhang, and A. Ma, *Investigation into the fatigue damage process of rubberized concrete and plain concrete by AE analysis*, Journal Of Materials In Civil Engineering 23 (7) (2010) 953-960.

[19] F. Liu, L.-y. Meng, G.-F. Ning, and L.-J. Li, *Fatigue performance of rubber-modified recycled aggregate concrete (RRAC) for pavement*, Construction and Building Materials 95 (2015) 207-217.

[20] N. Ganesan, J.B. Raj, and A. Shashikala, *Flexural fatigue behavior of self compacting rubberized concrete*, Construction and Building Materials 44 (2013) 7-14.

[21] F. Hernández-Olivares, G. Barluenga, B. Parga-Landa, M. Bollati, and B. Witoszek, *Fatigue behaviour of recycled tyre rubber-filled concrete and its implications in the design of rigid pavements*, Construction and Building Materials 21 (10) (2007) 1918-1927.

[22] T. Gupta, A. Tiwari, S. Siddique, R.K. Sharma, and S. Chaudhary, *Response Assessment under Dynamic Loading and Microstructural Investigations of Rubberized Concrete*, Journal Of Materials In Civil Engineering 29 (8) (2017) 04017062.

[23] I. Mohammadi, H. Khabbaz, and K. Vessalas, *In-depth assessment of Crumb Rubber Concrete (CRC) prepared by water-soaking treatment method for rigid pavements*, Construction and Building Materials 71 (2014) 456-471.

[24] A. Turatsinze, J.L. Granju, and S. Bonnet, *Positive synergy between steel-fibres and rubber aggregates: Effect on the resistance of cement-based mortars to shrinkage cracking*, Cement And Concrete Research 36 (9) (2006) 1692-1697.

[25] J.-h. Xie, Y.-c. Guo, L.-s. Liu, and Z.-h. Xie, *Compressive and flexural behaviours of a new steel-fibre-reinforced recycled aggregate concrete with crumb rubber*, Construction and Building Materials 79 (2015) 263-272.

[26] N.F. Medina, D.F. Medina, F. Hernández-Olivares, and M. Navacerrada, *Mechanical and thermal properties of concrete incorporating rubber and fibres from tyre recycling*, Construction and Building Materials 144 (2017) 563-573.

[27] A. Turatsinze, S. Bonnet, and J.-L. Granju, *Mechanical characterisation of cement-based mortar incorporating rubber aggregates from recycled worn tyres*, Building and environment 40 (2) (2005) 221-226.

[28] BSI, *EN 13877-1. Concrete pavements Part 1: Materials. BSI 389 Chiswick High Road London W4 4AL UK*, (2013).

[29] A. Alsaif, S.A. Bernal, M. Guadagnini, and K. Pilakoutas, *Durability of steel fibre reinforced rubberised concrete exposed to chlorides*, Construction and Building Materials 188 (2018) 130-142.

[30] A. Alsaif, S.A. Bernal, M. Guadagnini, and K. Pilakoutas, *Freeze-thaw resistance of steel fibre reinforced rubberised concrete*, Construction and Building Materials 195 (2019) 450-458.

[31] V. Baroghel-Bouny. *Evaluation and prediction of reinforced concrete durability by means of durability indicators. Part I: new performance-based approach*. in *ConcreteLife'06-International RILEM-JCI Seminar on Concrete Durability and Service Life Planning: Curing, Crack Control, Performance in Harsh Environments*. 2006: RILEM Publications SARL.

[32] M. Alexander, J. Mackechnie, and Y. Ballim, *Guide to the use of durability indexes for achieving durability in concrete structures*, Research monograph 2 (1999).

[33] Swedish standards, *SS 13 72 44 ED. 4.Concrete Testing - Hardened Concrete - Scaling At Freezing. Standardiserings-Kommissionen I Sverige*, (2005).

[34] RILEM, *TC 176-IDC: Internal damage of concrete due to frost action, Final Recommendation, Prepared by L. Tang and P.-E. Petersson SP Swedish National Testing and Research Institute, Boras, Sweden. Materials and Structures / Mat6riaux et Constructions, Vol. 37,December 2004, pp 754-759* in *Slab test: Freeze/thaw resistance of concreteInternal deterioration* 2004.

[35] ETRA, *The European Tyre Recycling Association*. 2016, Available at: http://www.etra-eu.org [Last accessed: 02/01/2018].

[36] S. Goel, S. Singh, and P. Singh, *Fatigue analysis of plain and fiber-reinforced self-consolidating concrete*, Materials Journal 109 (5) (2012) 573-582.

[37] B.H. Oh, *Fatigue analysis of plain concrete in flexure*, Journal of structural engineering 112 (2) (1986) 273-288.

[38] H. Hu, P. Papastergiou, H. Angelakopoulos, M. Guadagnini, and K. Pilakoutas, *Mechanical properties of SFRC using blended manufactured and recycled tyre steel fibres*, Construction and Building Materials 163 (2018) 376-389.

[39] ASTM, *C136: Standard test method for sieve analysis of fine and coarse aggregates. ASTM International, West Conshohocken, PA. doi:10.1520/C0136-06.* 2006.

[40] BSI, *EN 12390-2: Testing hardened concrete, Part 2: Making and curing specimens for strength tests. BSI 389 Chiswick High Road, London W4 4AL, UK.* 2009.

[41] BSI, *EN 12390-3: Testing hardened concrete, Part3: Compressive strength of test specimens. BSI 389 Chiswick High Road, London W4 4AL, UK.* 2009.
[42] JSCE, *SF-4: Method of test for flexural strength and flexural toughness of steel fiber reinforced concrete. Japan Concrete Institute, Tokio, Japan.*, (1984).
[43] S. Singh and S. Kaushik, *Flexural fatigue life distributions and failure probability of steel fibrous concrete*, Materials Journal 97 (6) (2000) 658-667.
[44] S. Singh, B. Ambedkar, Y. Mohammadi, and S. Kaushik, *Flexural fatigue strength prediction of steel fibre reinforced concrete beams*, Electronic Journal of Structural Engineering 8 (1) (2008) 46-54.
[45] RILEM, *TC 162-TDF: Test and design methods for steel fibre reinforced concrete, Bending test, Final Reccomendation. Materials and Structures: 35, 579-582.* 2002.
[46] B. Zhang, D. Phillips, and K. Wu, *Effects of loading frequency and stress reversal on fatigue life of plain concrete*, Magazine of Concrete Research 48 (177) (1996) 361-375.
[47] M. Darter and E. Barenberg, *DESIGN OF ZERO MAINTENANCE PLAIN JOINTED CONCRETE PAVEMENT, VOLUME TWO-DESIGN MANUAL*. 1977.
[48] J.R. Roesler, *Fatigue of concrete beams and slabs*. 1998.
[49] S. Singh and S. Kaushik, *Fatigue strength of steel fibre reinforced concrete in flexure*, Cement and Concrete Composites 25 (7) (2003) 779-786.
[50] B.H. Oh, *Fatigue life distributions of concrete for various stress levels*, Materials Journal 88 (2) (1991) 122-128.
[51] Y. Mohammadi and S. Kaushik, *Flexural fatigue-life distributions of plain and fibrous concrete at various stress levels*, Journal Of Materials In Civil Engineering 17 (6) (2005) 650-658.
[52] S. Singh, B. Singh, and S. Kaushik, *Probability of fatigue failure of steel fibrous concrete*, Magazine of Concrete Research 57 (2) (2005) 65-72.
[53] J.T. McCall. *Probability of fatigue failure of plain concrete*. in *Journal Proceedings*. 1958.
[54] H. Westergaard, *Stresses in concrete pavements computed by theoretical analysis*, Public roads (1926).
[55] G. Garber, *Design and construction of concrete floors*. 2006: CRC Press.
[56] TR34, *The Concrete Society: Concrete industrial ground floors – a guide to design and construction. 4rd ed. Technical Report 34; 2013.*
[57] Abaqus, *6.14 Abaqus Theory Manual. USA:Dassault Systemes Simulia Corporation*, 651 (2014).
[58] J. Hua, *Finite element modeling and analysis of accelerated pavement testing devices and rutting phenomenon*, (2000).
[59] I. ARA, ERES Consultants Division., *Guide for Mechanistic–Empirical Design of New and Rehabilitated Pavement Structures*, Final Rep., NCHRP Project 1-37A (2004).
[60] H. Jiang and Y. Xie, *A note on the Mohr–Coulomb and Drucker–Prager strength criteria*, Mechanics Research Communications 38 (4) (2011) 309-314.
[61] N. Jafarifar, K. Pilakoutas, H. Angelakopoulos, and T. Bennett, *Post-cracking tensile behaviour of steel-fibre-reinforced roller-compacted-concrete for FE modelling and design purposes*, (2017).
[62] P. Casanova and P. Rossi, *Analysis and design of steel fiber reinforced concrete beams*, Structural Journal 94 (5) (1997) 595-602.
[63] N. Jafarifar, K. Pilakoutas, and T. Bennett, *Moisture transport and drying shrinkage properties of steel–fibre-reinforced-concrete*, Construction and Building Materials 73 (2014) 41-50.
[64] B. Mobasher, *Mechanics of fiber and textile reinforced cement composites*. 2011: CRC press.